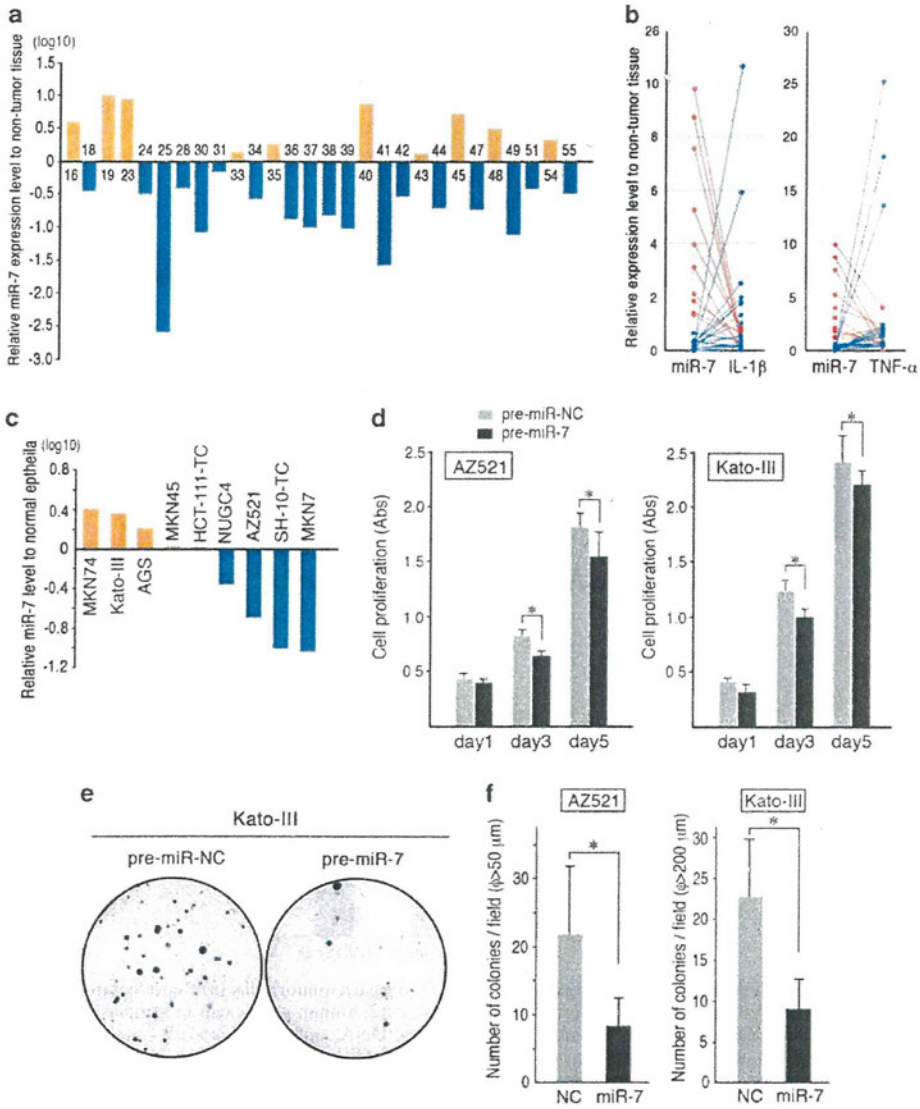

Figure 3 The tumor-suppressor roles of miR-7 in gastric cancer cells. (**a**) The relative miR-7 expression levels in the human gastric cancer tissue samples to the level of non-tumor stomach tissue samples are shown as the log10 ratios. The indicated numbers correspond to the patient ID in the clinicopathological data (Supplementary Table 3). (**b**) Comparison of the relative expression levels of miR-7 and IL-1β (left) or TNF-α (right) in gastric cancer tissues to the non-tumor stomach tissue levels in each patient is shown. Red and blue lines indicate that the expression of miR-7 was increased (>1.0) and decreased (<1.0) in the gastric cancers, respectively. (**c**) The relative expression levels of miR-7 in gastric cancer cell lines compared with the mean level in the human normal gastric epithelial cells are shown as the log10 ratios. The expression levels of miR-7 were normalized to those of U44. (**d**) The proliferation of control (gray bars) and pre-miR-7-transfected (closed bars) AZ521 cells and Kato-III cells at the indicated culture days are shown (mean ± s.d.). $*P<0.05$. (**e**) Representative photographs of soft agar colonies in 6-well plates showing the pre-miR-NC- (left) and pre-miR-7-transfected (right) Kato-III cells. (**f**) The mean numbers of soft agar colonies larger than the indicated diameters in each well of 6-well plate of control (gray bars) and pre-miR-7-transfected (closed bars) AZ521 cells and Kato-III cells are shown (mean ± s.d.). $*P<0.05$.

the upstream CpG islands of *Hnrnpk*. However, the H3K27me3 level was not increased in mouse gastritis and gastric tumors compared with the wild-type stomach (Figure 4b). These results indicate that DNA methylation and trimethylation of H3K27 are not involved in the downregulation of miR-7-1. Moreover, the genomic region including miR-7-1 was not deleted in human gastric cancer cells (Supplementary Figure 3b), suggesting that miR-7 downregulation in gastric cancer is not caused by genomic deletion.

We next examined whether activated macrophages have a role in the downregulation of miR-7, because the major source of proinflammatory cytokines in gastric tumors are macrophages (Oshima *et al.*, 2004, 2011). To monitor miR-7 activity, reporter vector-transfected cells were used. We confirmed that luciferase activity

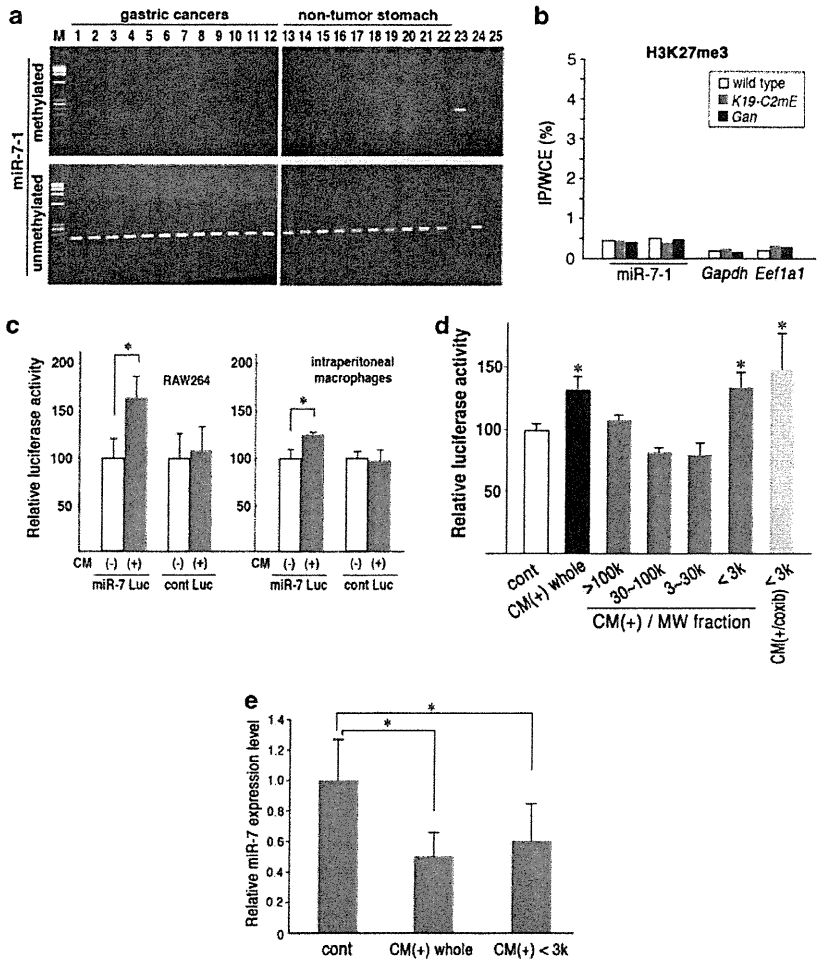

Figure 4 The mechanism responsible for the downregulation of miR-7 in gastric tumor cells. (**a**) Representative results of methylated (top) or unmethylated (bottom) status-specific PCR for miR-7-1. Lanes 1–12, human gastric cancer samples; lanes 13–22, non-tumor stomach samples; lane 23, methylated DNA control; lane 24, unmethylated DNA control; and lane 25, water control. (**b**) The results of ChIP-PCR analyses of miR-7-1 and the housekeeping genes, *Gapdh* and *Eef1a1*, for H3K27me3 in the gastric mucosa of respective genotype mice. The percentages of immunoprecipitated (*IP*)/whole-cell extracts (*WCE*) are shown for each primer set. (**c**) The luciferase activities of miR-7 Luc- or control Luc-transfected AZ521 reporter cells stimulated with CM(+) (gray bars) relative to those with CM(−) (open bars) are shown (mean ± s.d.). $*P<0.05$. The conditioned medium was prepared from RAW264 cells (left) or intraperitoneal macrophages (right). (**d**) The luciferase activities of miR-7 Luc-transfected AZ521 reporter cells stimulated with whole CM(+) (closed bars), CM(+) fractionated to the indicated molecular sizes (gray bars), or fractionated CM(+) to <3 kDa collected from celecoxib-treated and LPS-stimulated macrophages (light gray bar) relative to the control level (open bar) are shown (mean ± s.d.). $*P<0.05$ versus the control level. (**e**) The relative miR-7 expression levels examined by real-time RT–PCR in AZ521 cells stimulated with whole CM(+) or fractioned CM(+) <3 kDa relative to the control level are shown (mean ± s.d.). $*P<0.05$ versus the control level. The expression levels of miR-7 were normalized to the U44 level.

was increased significantly when the miR-7 inhibitor was transfected into reporter vector-transfected Kato-III cells (Supplementary Figure 1c), indicating that the luciferase reporter system was working. Reporter cells were then treated with the conditioned medium of lipopolysaccharide-stimulated RAW264 cells (CM(+)) or unstimulated RAW264 cells (CM(−)). Importantly, the luciferase activity increased significantly when cells were stimulated with CM(+), whereas the luciferase activity was not changed in control vector-transfected cells (Figure 4c). Similar results were obtained when CM(+) and CM(−) were prepared using mouse intraperitoneal macrophages. These results indicate that activated macrophage-derived factor(s) caused miR-7 downregulation in gastric cancer cells.

To identify macrophage-derived factor(s) that suppress miR-7 expression, reporter cells were stimulated with TNF-α, IL-1β, IL-6 or PGE_2. However, none of these factors caused an increase in luciferase activity (Supplementary Figure 4). We thus fractionated CM(+) by ultrafiltration, and separated by molecular weight. Interestingly, a CM(+) fraction of <3 kDa significantly increased the luciferase activity to a similar level as that induced by whole CM(+), whereas the other CM(+) fractions did not (Figure 4d). Moreover, the luciferase activity was still increased when CM(+)

was prepared under co-treatment of RAW264 cells with lipopolysaccharide and a COX-2 inhibitor, celecoxib. We confirmed the decreased level of miR-7 by real-time RT–PCR in CM(+)- or CM(+) fraction <3 kDa-treated AZ521 cells (Figure 4e). These results indicate that small molecule(s) (<3 kDa) derived from activated macrophages are responsible for miR-7 repression in gastric cancer cells, and that such small molecule(s) are expressed in activated macrophages in a COX-2/PGE_2-independent manner.

Downregulation of miR-7 in the stomach by inflammatory responses

We next examined whether inflammatory responses are responsible for miR-7 downregulation in the stomach using different mouse models. The stomachs of wild-type mice were infected with *Helicobacter felis*, and submucosal inflammatory infiltration and mucosal macrophage accumulation were confirmed at 20 weeks after the infection (Figures 5a and b). Notably, the miR-7 expression level was significantly decreased in the *H. felis*-infected inflamed gastric mucosa (Figure 5c).

We recently showed that inflammatory responses and macrophage infiltration were suppressed in *K19-C2mE* mouse gastritis and *Gan* mouse tumors when mice were maintained under germfree conditions (Figure 5d and Oshima *et al.*, 2011). Notably, miR-7 expression levels were increased significantly in germfree *K19-C2mE* and *Gan* mice compared with the levels of mice maintained in a specific pathogen free (SPF) facility (Figure 5e). These *in vivo* experiments suggest that inflammatory responses are responsible for the miR-7 downregulation in the stomach, although further genetic studies are required to examine the role of macrophages in miR-7 downregulation.

Inflammation-dependent upregulation of miR-7 target genes in gastric tumors

The epidermal growth factor receptor (*EGFR*) mRNA is one of the miR-7 target genes (Kefas *et al.*, 2008;

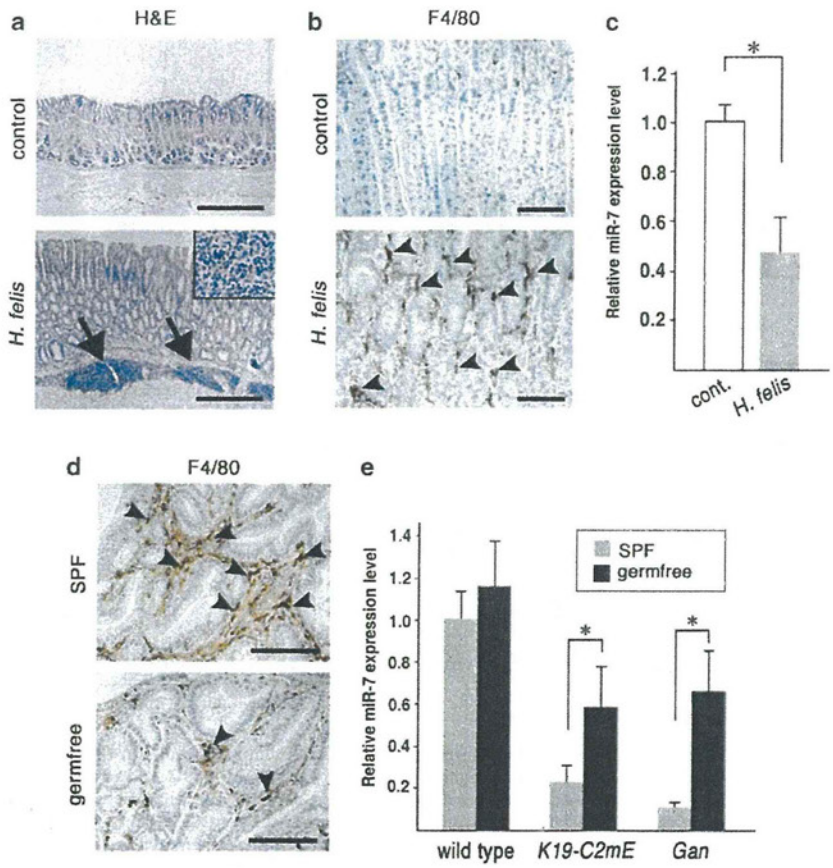

Figure 5 Inflammation-induced miR-7 repression in the mouse stomachs. (**a**) Histology of the wild-type mouse normal glandular stomach (top) and *H. felis*-infected inflamed glandular stomach (bottom). Arrows and inset indicate submucosal inflammatory cell infiltration. Scale bars indicate 0.5 mm. (**b**) Immunostaining of F4/80 in the normal glandular stomach (top) and *H. felis*-infected glandular stomach (bottom). Arrowheads indicate macrophages. Scale bars indicate 100 μm. (**c**) The miR-7 expression level of *H. felis*-infected gastric mucosa (gray bar) relative to that of the control stomach (open bar) is shown (mean ± s.d.). $*P<0.05$. (**d**) Immunostaining of F4/80 in a SPF control *Gan* mouse tumor (top) and a germfree *Gan* mouse tumor (bottom). Arrowheads indicate macrophages. Scale bars indicate 100 μm. (**e**) The expression levels of miR-7 in SPF (gray bars) and germfree (closed bars) K19-*C2mE* mouse gastritis and *Gan* mouse gastric tumors relative to the SPF wild-type stomach levels are shown (mean ± s.d.). $*P<0.05$. The expression levels of miR-7 were normalized to the Sno202 level.

Webster *et al.*, 2009). We thus examined *EGFR* expression levels in pre-miR-7-transfected Kato-III and AZ521 gastric cancer cells. As expected, the *EGFR* expression level was decreased significantly by pre-miR-7 transfection in both cell lines (Figure 6a), suggesting that suppression of *EGFR* expression is one of the tumor-suppressor mechanisms of miR-7 against gastric cancer development.

To identify novel miR-7 target genes that are upregulated in the inflammatory microenvironment,

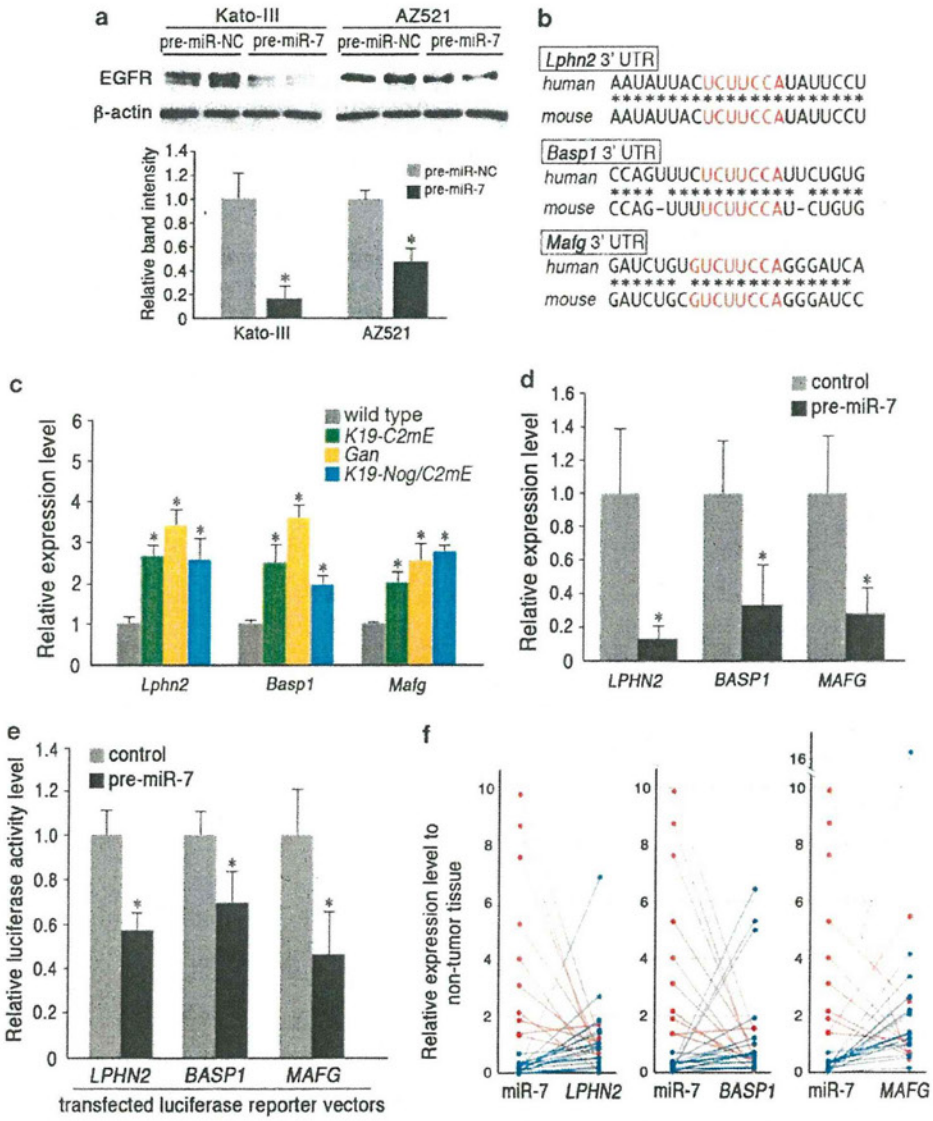

Figure 6 Inflammation-dependent upregulation of miR-7 target genes. (**a**) Representative results of the western blotting analysis of EGFR in Kato-III cells (top left) and AZ521 cells (top right) transfected with pre-miR-NC and pre-miR-7. The results for two independently prepared samples are shown. β-Actin was used as an internal control. The relative band intensities of the western blotting results are shown in the bar graph (mean ± s.d.) (bottom). $*P<0.05$ versus the control level. (**b**) Alignment of the miR-7 target sequences in the 3′-UTR of *Lphn2*, *Basp1* and *Mafg* in human and mouse mRNAs. The seed match sequences for miR-7 are indicated in red. (**c**) The expression levels of the indicated genes in *K19-C2mE* mouse gastritis (green bars), *Gan* mouse gastric tumors (yellow bars) and *K19-Nog/C2mE* mouse gastric hamartomas (blue bars) relative to the wild-type levels (gray bars) are shown (mean ± s.d.). $*P<0.05$ versus the wild-type level. The results were extracted from the microarray data set (Gene Expression Omnibus (GEO), accession GSE16902). (**d**) The expression levels of the indicated genes examined by real-time RT–PCR in pre-miR-7-transfected Kato-III cells (closed bar) relative to those of the control cells (gray bar) are shown (mean ± s.d.). $*P<0.05$ versus control level. (**e**) The relative luciferase activity levels of pre-miR-7-transfected reporter cells (closed bars) to the levels of control pre-miR-NC-transfected reporter cells (gray bars) are shown. The target genes for the respective luciferase reporter vectors are indicated. $*P<0.05$ versus the control level. (**f**) Comparison of the relative expression levels of miR-7 and *LPHN2* (left), *BASP1* (center) or *MAFG* (right) in human gastric cancers with non-tumor stomach levels is shown. Red and blue lines indicate that miR-7 was increased (>1.0) and decreased (<1.0) in gastric cancers, respectively. The expression levels of miR-7 were normalized to the U44 level.

we searched for putative miR-7 target genes from the upregulated gene set in both *K19-C2mE* mouse gastritis and *Gan* mouse gastric tumors using the results of the microarray analyses (Itadani *et al.*, 2009). We found that the *Lphn2*, *Basp1* and *Mafg* genes have conserved miR-7 target sequences in their 3′ untranslated region in both mouse and human mRNAs (Figure 6b). Notably, the expression of these genes was significantly increased not only in *K19-C2mE* mouse gastritis and *Gan* mouse tumors but also in *K19-Nog/C2mE* mouse gastric hamartomas (Figure 6c). The gastric mucosa and tumors in these strains are inflamed as a result of induction of the COX-2/PGE_2 pathway (Oshima *et al.*, 2004, 2006, 2009), suggesting that downregulation of miR-7 in inflammatory lesions is involved in upregulation of these genes. Notably, transfection of pre-miR-7 into Kato-III cells resulted in a significant decrease of *LPHN2*, *BASP1* and *MAFG* expressions (Figure 6d). Moreover, we constructed luciferase reporter plasmids that contained the 3′ untranslated region fragment of the putative miR-7 target genes, and transfected these vectors into Kato-III cells. Consistent with the real-time RT–PCR results, luciferase activities of reporter vector-transfected cells decreased significantly when cells were co-transfected with pre-miR-7 (Figure 6e). Taken together, these results indicate that these three genes are miR-7 targets.

Finally, we examined the expressions of *LPHN2*, *BASP1* and *MAFG* in human gastric cancers by real-time RT–PCR and compared their expressions with miR-7 expression levels. We found that expression levels of miR-7 and *LPHN2*, *BASP1* and *MAFG* were inversely correlated (Figure 6f). Accordingly, it is possible that inflammation causes induction of these genes in human gastric cancers through downregulation of miR-7, which may contribute to gastric tumorigenesis, although this will need to be investigated in future studies.

Discussion

It has been shown that miR-155 and miR-21, which function as oncogenes, are induced by inflammatory pathways, providing a link between inflammation and cancer (O'Connell *et al.*, 2007; Tili *et al.*, 2007; Iliopoulos *et al.*, 2010). Consistently, we found inflammation-dependent induction of miR-155 and miR-21 in mouse gastric tumors. On the other hand, miR-145 and miR-7, which function as tumor suppressors, are downregulated in both mouse gastritis and gastric tumor tissues. Moreover, we found that miR-7 levels are inversely correlated with the levels of proinflammatory cytokines, suggesting that the severity of inflammatory response is related to miR-7 downregulation. Therefore, it is possible that inflammation can promote tumorigenesis both by the upregulation of oncogenic miRNAs and by the downregulation of tumor-suppressor miRNAs, possibly through different mechanisms. Such alterations of cancer-related miRNA expression likely link inflammation and cancer.

It has been reported that miR-7 has a tumor-suppressor role in various cancers including brain tumors, breast cancer and lung cancer (Kefas *et al.*, 2008; Reddy *et al.*, 2008; Webster *et al.*, 2009), and we herein showed that miR-7 also functions as a tumor suppressor in gastric cancer. Interestingly, in the normal stomach, miR-7 expression is induced during the differentiation of gastric epithelial cells, suggesting a role of miR-7 in the regulation of epithelial cell differentiation. It has also been reported that miR-7 expression is induced during differentiation of intestinal epithelial cells (Nguyen *et al.*, 2010) and cortical neurons (Chen *et al.*, 2010). These results collectively suggest that miR-7 has a role in regulating cell differentiation in various organs. Therefore, it is conceivable that suppression of miR-7 expression is required for maintenance of the undifferentiated status of stem or progenitor cells in these organs.

These results suggest the possibility that inflammation suppresses epithelial cell differentiation through repression of miR-7. It is not surprising that the inflammatory response suppresses cell differentiation and enhances proliferation when regeneration is required in injured tissues. It has also been shown that a disruption of Toll-like receptor signaling causes an impairment of tissue repair by intestinal epithelial cells (Rakoff-Nahoum *et al.*, 2004). Moreover, activated macrophages are important niche components for intestinal epithelial progenitors in regenerative responses (Pull *et al.*, 2005). Therefore, it is conceivable that downregulation of miR-7 leads to suppression of differentiation, inducing the proliferation of undifferentiated epithelial cells in the inflammatory microenvironment.

Although several target genes of miR-7 have been identified, it is still unclear how miR-7 regulates differentiation. *EGFR* is one of the important miR-7 target genes, and is at least partially responsible for its tumor-suppressor role (Kefas *et al.*, 2008). Moreover, p21-activated kinase 1, Raf1, and the insulin-like growth factor 1 receptor have also been identified as miR-7 target genes that are upregulated in cancer cells (Reddy *et al.*, 2008; Webster *et al.*, 2009; Jiang *et al.*, 2010). Although most of these gene products contribute to cancer cell proliferation, we believe that miR-7 inhibits expression of other factors that have a role in the maintenance of the undifferentiated status of epithelial cells. In this study, we identified three novel miR-7 target genes that are upregulated in gastric cancers in an inflammation-dependent manner. LPHN2 is a G protein-coupled receptor that binds α-latrotoxin (Ichtchenko *et al.*, 1999), whereas BASP1 is implicated in neurite outgrowth (Korshunova *et al.*, 2008). MAFG is one of the small Maf proteins that is important for antioxidant responses (Katsuoka *et al.*, 2005). Although it remains to be investigated, it is of interest to examine whether these molecules have any role in the differentiation or tumorigenesis of gastric epithelial cells.

We examined the mechanisms responsible for miR-7 downregulation in gastric tumor cells. *Helicobacter pylori* infection induces chronic gastritis, resulting in induction of DNA methylation (Niwa *et al.*, 2010). The

expression of miR-34b/c is suppressed by DNA methylation in *H. pylori*-associated gastric cancer cells (Suzuki *et al.*, 2010). Moreover, H3K27me3 leads to tumor-suppressor gene silencing in cancer (Kondo *et al.*, 2008). However, we showed that downregulation of miR-7 is not caused by genomic deletion nor by epigenetic mechanisms, but through stimulation by macrophage-derived factor(s). Several mechanisms for the regulation of miR-7 expression have been reported. For example, miR-7 transcription is directly induced by HoxD10 (Reddy *et al.*, 2008) or c-Myc (Chou *et al.*, 2010). Splicing factor SF2/ASF binds the pri-miR-7 to enhance its cleavage by Drosha (Wu *et al.*, 2010). Accordingly, it is conceivable that macrophage-derived molecule(s) directly downregulate miR-7 expression or indirectly suppress miR-7 expression through modulation of these regulation systems. The identification of responsible macrophage-derived molecule(s) will provide a novel mechanism by which macrophages promote tumorigenesis.

In conclusion, we showed that inflammation simultaneously induces upregulation of oncogenic miRNAs and downregulation of tumor-suppressor miRNAs, which promote tumorigenesis. The expression of miR-7 is induced during differentiation of gastric epithelial cells, suggesting a role for miR-7 in the regulation of epithelial cell differentiation. Accordingly, it is possible that the downregulation of miR-7 contributes to suppression of differentiation, resulting in the promotion of gastric tumorigenesis. Moreover, small molecule(s) expressed by activated macrophages are responsible for miR-7 repression, providing a link between inflammation and cancer. Therefore, miR-7 may be useful for devising a new preventive or therapeutic strategy against gastric cancer through the induction of cancer cell differentiation.

Materials and methods

Mouse models

Construction of *K19-C2mE* and *Gan* (*K19-Wnt1/C2mE*) mice was described previously (Oshima *et al.*, 2004, 2006). In brief, *K19-C2mE* mice express *Ptgs2* and *Ptges* in gastric epithelial cells, whereas *Gan* mice express *Ptgs2*, *Ptges* and *Wnt1*. For expression analyses, *K19-C2mE* mouse gastritis and *Gan* mouse gastric tumor samples, and wild-type mouse stomach tissues were obtained at 30–40 weeks of age. Germfree mouse colonies were constructed as described previously (Oshima *et al.*, 2011), and the histology and miR-7 expression were examined at 55 weeks of age ($n=5$). *H. felis* (American Type Culture Collection 49179, ATCC, Manassas, VA, USA) were inoculated at 10^8 per mouse into wild-type mice at 6–8 weeks of age, and the histology and miRNA expression were examined at 20 weeks after infection ($n=6$). All animal experiments were carried out according to a protocol approved by the Committee on Animal Experimentation of the Kanazawa University.

Microarray analysis

Total RNA was extracted from mouse stomachs ($n=3$) using ISOGEN (Nippon Gene, Tokyo, Japan), pooled with the same genotype mouse RNAs, labeled with Cy3 and hybridized to Mouse miRNA microarray Rel. 12.0 (Agilent Technologies, Santa Clara, CA, USA). The raw data were normalized using the GeneSpring GX software program (Agilent Technologies), and expression levels of miRNAs in gastritis and gastric tumor tissues were compared with those in the wild-type mouse stomach. Transcripts with low signals (less than threefold of the background level) were not used for further analyses. The expression of miRNAs was further examined by real-time RT–PCR using RNA samples independently prepared from a different set of wild-type, *K19-C2mE* and *Gan* mice ($n=5$ for each genotype).

The results of cDNA microarray data sets of *K19-C2mE*, *Gan* and *K19-Nog/C2mE* mice were deposited into the Gene Expression Omnibus, as accession number GSE16902 (Itadani *et al.*, 2009), and were searched for the presence of novel miR-7 target genes using the TargetScan 5.1 program (MIT, Cambridge, MA, USA) (http://www.targetscan.org).

Real-time RT–PCR

Paired gastric cancer and non-tumor stomach tissue samples were obtained from 28 patients during surgery at the Kanazawa University Hospital, Japan. Fresh frozen tissues were used for expression analyses. Clinicopathological data of patients are shown in Supplementary Table 3. Human normal gastric epithelial cells were prepared by isolating the gastric glands from normal stomach tissues ($n=4$) as described previously (Cheng *et al.*, 1984). Approval for this project was obtained from the Kanazawa University Medical Ethics Committee, and written informed consent was obtained before specimen collection. Mouse stomachs were obtained from E15 wild-type mouse embryos, and day 0, day 7, day 14 and adult mice ($n=3$ for each). Total RNAs were extracted from tissues or cells using ISOGEN (Nippon Gene), and cDNAs for miRNAs and mRNAs were constructed using QuantiMir RT kit (System Bioscience, Mountain View, CA, USA) and the PrimeScript RT reagent Kit (Takara, Tokyo, Japan), respectively. Real-time RT–PCR was performed using SYBR Premix Ex TaqII (Takara, Tokyo, Japan) and Stratagene Mx3000P (Agilent Technologies). Sno202 and U44 were used as endogenous miRNA controls for mice and humans, respectively, whereas β-actin was used for endogenous mRNA control. The primer sequences for the miRNAs are shown in Supplementary Table 4. The primers for mRNAs were purchased from Takara.

Cell culture experiments

Mouse glandular stomachs were treated with 0.1% collagenase for 30 min at 37 °C, followed by centrifugation at 20 *g* for 3 min to isolate gastric glands. For the primary culture, isolated gastric glands were digested with trypsin and seeded on collagen-coated dishes as described previously (Oshima *et al.*, 2004). On day 2, the primary cultured cells were treated with 10 mM EDTA-phosphate-buffered saline and passaged. The primary cultured cells on day 2 (P0) and day 6 (P1) were used for the expression analysis. Human gastric cancer cell lines, AGS (ATCC), AZ521, MKN74, MKN45, NUGC4, HCT-111-TC, SH-10-TC (RIKEN BioResource Center, Tsukuba, Japan), Kato-III and MKN7 (Cell Resource Center for Biomedical Research, Tohoku University, Japan) were used in this study.

The pre-miR miRNA-7 (Pre-miR-7), pre-miR negative control (Pre-miR-NC) and anti-miR-7 inhibitor (Ambion, Austin, TX, USA) were used for transfection. The cell proliferation rate was measured using the Cell Counting Kit-8 (Dojindo, Kumamoto, Japan). For the soft agar colony

formation assay, cells were suspended in culture medium with 0.33% agar, and seeded in a 6-well plate. After 21 days of culture, soft agar was stained with Giemsa solution (Wako, Osaka, Japan).

Histological and immunohistochemical analyses
Tissues were fixed in 4% paraformaldehyde, embedded and sectioned at 4-μm thickness. Sections were stained with hematoxylin and eosin. Antibodies against Ki-67 (DakoCytomation, Carpenteria, CA, USA) and F4/80 (Serotec, Oxford, UK) were used as the primary antibodies. Immunostaining signals were visualized using the Vectastain Elite Kit (Vector Laboratories, Burlingame, CA, USA), and the MOM kit (Vector Laboratories) was used to minimize the background staining signals.

Methylation-specific PCR analysis
The methylation status of miR-7-1 in human gastric cancer and non-tumor tissues was examined by methylation-specific PCR analysis as described previously (Yamashita *et al.*, 2008). Methylation-specific PCR was performed with a primer set specific for the methylated or unmethylated sequence (Me or Un set in Supplementary Table 4). DNA methylated by SssI methylase (New England Biolabs, Ipswich, MA, USA) and DNA amplified by a GenomiPhi DNA amplification kit (GE Healthcare, Buckinghamshire, UK) were used as methylated and unmethylated controls, respectively.

Chromatin immunoprecipitation analyses
Histone modifications were examined by chromatin immunoprecipitation assay as described previously (Yamashita *et al.*, 2008; Takeshima *et al.*, 2009). In brief, gastric epithelial cells of wild-type, *K19-C2mE* and *Gan* mice ($n=3$ for each genotype) were cross-linked with 1% formaldehyde, and sheared chromatin by Bioruptor UCD-250 (Cosmo Bio, Tokyo, Japan). The samples were incubated with an antibody against H3K27me3 (07-449, Millipore, Billerica, MA, USA), and genomic DNA samples were used for the quantitative chromatin immunoprecipitation-PCR analyses. The primer set was designed for the upstream CpG islands of miR-7-1 (Supplementary Table 4).

Luciferase reporter assay
Constructions of the miR-7 luciferase reporter vector (miR-7 Luc) and control vector (control Luc) are shown in Supplementary Figure 1. Luciferase reporter vectors for the *LPHN2*, *BASP1* and *MAFG* genes were constructed by subcloning 3′ untranslated region fragments of the respective human genes into the pGL3 plasmid (Promega, Madison, WI, USA). PCR primer sequences for cloning 3′ untranslated region of the respective genes and amplified fragment lengths are indicated in Supplementary Table 4. The luciferase activity was measured using a Luciferase Assay System (Promega), and the levels were normalized to the total protein levels detected using the Pierce 660 nm Protein Assay (Thermo Scientific, Yokohama, Japan). RAW264 cells (RIKEN BioResource Center) and mouse intraperitoneal macrophages were stimulated with 10 ng/ml lipopolysaccharide (Sigma, St Louis, MO, USA) for 24 h and the conditioned medium was collected as CM(+). The conditioned medium of unstimulated macrophages was collected as CM(−). The conditioned medium of lipopolysaccharide-stimulated and COX-2 inhibitor celecoxib-treated (Pfizer, New York, NY, USA) (10 μM) RAW264 cells was collected as CM(+/coxib). CM(+) was fractionated by ultrafiltration using Centricon Plus-70 (Millipore) to prepare CM(+) >100 kDa, 30–100 kDa, 3–30 kDa and <3 kDa. Cells were stimulated with CM at a 50% concentration.

Western blotting analysis
Cells were transfected with pre-miR-7 or pre-miR-NC, lysed at 24 h after transfection, and 10 μg of protein was separated in 7.5% SDS-polyacrylamide gels. An antibody against EGFR (Cell Signaling Technology, Danvers, MA, USA) was used as the primary antibody. Anti-β-actin (Sigma) was used as an internal control. The ECL detection system (GE Healthcare) was used to detect the signals, and band intensities were quantified using the ImageJ application (NIH, Bethesda, MD, USA).

Statistical analysis
The data were analyzed by the unpaired *t*-test using the Microsoft Excel software program (Microsoft). A value of $P<0.05$ was considered to be statistically significant.

Conflict of interest

The authors declare no conflict of interest.

Acknowledgements

We thank Manami Watanabe for her excellent technical assistance. This work was supported by Grants-in-Aid from the Ministry of Education, Culture, Sports, Science and Technology of Japan, and the Ministry of Health, Labour and Welfare of Japan.

References

Ambros V. (2004). The functions of animal microRNAs. *Nature* **431**: 350–355.

Bartel DP. (2004). MicroRNAs: genomics, biogenesis, mechanism, and function. *Cell* **116**: 281–297.

Chen H, Shalom-Feuerstein R, Riley J, Zhang SD, Tucci P, Agostini M *et al.* (2010). miR-7 and miR-214 are specifically expressed during neuroblastoma differentiation, cortical development and embryonic stem cells differentiation, and control neurite outgrowth *in vitro*. *Biochem Biophys Res Commun* **394**: 921–927.

Cheng H, Bjerknes M, Amar J. (1984). Methods for the determination of epithelial cell kinetic parameters of human colonic epithelium isolated from surgical and biopsy. *Gastroenterology* **86**: 78–85.

Chou YT, Lin HH, Lien YC, Wang YH, Hong CF, Kao YR *et al.* (2010). EGFR promotes lung tumorigenesis by activating miR-7 through a Ras/ERK/Myc pathway that targets the Ets2 transcriptional repressor ERF. *Cancer Res* **70**: 8822–8831.

Coussens LM, Werb Z. (2002). Inflammation and cancer. *Nature* **420**: 860–867.

Di Leva G, Croce CM. (2010). Roles of small RNAs in tumor formation. *Trends Mol Med* **16**: 257–267.

Esquela-Kerscher A, Slack FJ. (2006). Oncomirs-microRNAs with a role in cancer. *Nat Rev Cancer* **6**: 259–269.

Ichtchenko K, Bittner MA, Krasnoperov V, Little AR, Chepurny O, Holz RW *et al.* (1999). A novel ubiquitously expressed α-latrotoxin

receptor is a member of the CIRL family of G-protein-coupled receptors. *J Biol Chem* **274**: 5491–5498.

Iliopoulos D, Jaeger SA, Hirsch HA, Bulyk ML, Struhl K. (2010). STAT3 activation of miR-21 and miR-181b-1 via PTEN and CYLD are part of the epigenetic switch linking inflammation to cancer. *Mol Cell* **39**: 493–506.

Itadani H, Oshima H, Oshima M, Kotani H. (2009). Mouse gastric tumor models with prostaglandin E_2 pathway activation show similar gene expression profiles to intestinal-type human gastric cancer. *BMC Genomics* **10**: 615.

Jiang L, Liu X, Chen Z, Jin Y, Heidbreder CE, Kolokythas A *et al.* (2010). MicroRNA-7 targets IGF1R (insulin-like growth factor 1 receptor) in tongue squamous cell carcinoma cells. *Biochem J* **432**: 199–205.

Katsuoka F, Motohashi H, Ishii T, Aburatani H, Engel JD, Yamamoto M. (2005). Genetic evidence that small maf proteins are essential for the activation of antioxidant response element-dependent genes. *Mol Cell Biol* **25**: 8044–8051.

Kefas B, Godlewski J, Comeau L, Li Y, Abounader R, Hawkinson M *et al.* (2008). MicroRNA-7 inhibits the epidermal growth factor receptor and the Akt pathway and is down-regulated in glioblastoma. *Cancer Res* **68**: 3566–3572.

Kondo Y, Shen L, Cheng AS, Ahmed S, Boumber Y, Charo C *et al.* (2008). Gene silencing in cancer by histone H3 lysine 27 trimethylation independent of promoter methylation. *Nat Genet* **40**: 741–750.

Korshunova I, Caroni P, Kolkova K, Berezin V, Bock E, Walmod PS. (2008). Characterization of BASP-1 mediated neurite outgrowth. *J Neurosci Res* **86**: 2201–2213.

Niwa T, Tsukamoto T, Toyoda T, Mori A, Tanaka H, Maekita T *et al.* (2010). Inflammatory processes triggered by *Helicobacter pylori* infection cause aberrant DNA methylation in gastric epithelial cells. *Cancer Res* **70**: 1430–1440.

Nguyen HT, Dalmasso G, Yan Y, Laroui H, Dahan S, Mayer L *et al.* (2010). MicroRNA-7 modulates CD98 expression during intestinal epithelial cell differentiation. *J Biol Chem* **285**: 1479–1489.

O'Connell RM, Taganov KD, Boldin MP, Cheng G, Baltimore D. (2007). MicroRNA-155 is induced during the macrophage inflammatory response. *Proc Natl Acad Sci USA* **104**: 1604–1609.

Oshima H, Hioki K, Popivanova BK, Oguma K, van Rooijen N, Ishikawa TO *et al.* (2011). Prostaglandin E_2 signaling and bacterial infection recruit tumor-promoting macrophages to mouse gastric tumors. *Gastroenterology* **140**: 596–607.

Oshima H, Itadani H, Kotani H, Taketo MM, Oshima M. (2009). Induction of prostaglandin E_2 pathway promotes gastric hamartoma development with suppression of bone morphogenetic protein signaling. *Cancer Res* **69**: 2729–2733.

Oshima H, Matsunaga A, Fujimura T, Tsukamoto T, Taketo MM, Oshima M. (2006). Carcinogeniesis in mouse stomach by simultaneous activation of the Wnt signaling and prostaglandin E_2 pathway. *Gastroenterology* **131**: 1086–1095.

Oshima H, Oshima M, Inaba K, Taketo MM. (2004). Hyperplastic gastric tumors induced by activated macrophages in COX-2/mPGES-1 transgenic mice. *EMBO J* **23**: 1669–1678.

Pull SL, Doherty JM, Mills JC, Gordon JI, Stappenbeck TS. (2005). Activated macrophages are an adaptive element of the colonic epithelial progenitor niche necessary for regenerative responses to injury. *Proc Natl Acad Sci USA* **102**: 99–104.

Rakoff-Nahoum S, Paglino J, Eslami-Varzaneh F, Edberg S, Medzhitov R. (2004). Recognition of commensal microflora by Toll-like receptors is required for intestinal homeostasis. *Cell* **118**: 229–241.

Reddy SD, Ohshiro K, Rayala SK, Kumar R. (2008). MicroRNA-7, a homeobox D10 target, inhibits p21-activated kinase 1 and regulates its functions. *Cancer Res* **68**: 8195–8200.

Sachdeva M, Zhu S, Wu F, Wu H, Walia V, Kumar S *et al.* (2009). p53 represses c-Myc through induction of the tumor suppressor miR-145. *Proc Natl Acad Sci USA* **106**: 3207–3212.

Saydam O, Senol O, Wurdinger T, Mizrak A, Ozdener GB, Stemmer-Rachamimov AO *et al.* (2011). miRNA-7 attenuation in Schwannoma tumors stimulates growth by upregulating three oncogenic signaling pathways. *Cancer Res* **71**: 852–861.

Sonkoly E, Pivarcsi A. (2011). MicroRNAs in inflammation and response to injuries induced by environmental pollution. *Mutat Res* **717**: 46–53.

Sonoshita M, Takaku K, Sasaki N, Sugimoto Y, Ushikubi F, Narumiya S *et al.* (2001). Acceleration of intestinal polyposis through prostaglandin receptor EP2 in $Apc^{\Delta 716}$ knockout mice. *Nat Med* **7**: 1048–1051.

Suzuki H, Yamamoto E, Nojima M, Kai M, Yamano H, Yoshikawa K *et al.* (2010). Methylation-associated silencing of microRNA-34b/c in gastric cancer and its involvement in an epigenetic field defect. *Carcinogenesis* **31**: 2066–2073.

Takeshima H, Yamashita S, Shimazu T, Niwa T, Ushijima T. (2009). The presence of RNA polymerase II, active or stalled, predicts epigenetic fate of promoter CpG islands. *Genome Res* **19**: 1974–1982.

Tili E, Michaille JJ, Cimino A, Costinean S, Dumitru CD, Adair B *et al.* (2007). Modulation of miR-155 and miR-125b levels following lipopolysaccharide/TNF-α stimulation and their possible roles in regulating the response to endotoxin shock. *J Immunol* **179**: 5082–5089.

Ventura A, Jacks T. (2009). MicroRNAs and cancer: short RNAs go a long way. *Cell* **136**: 586–591.

Volinia S, Calin GA, Liu CG, Ambs S, Cimmino A, Petrocca F *et al.* (2006). A microRNA expression signature of human solid tumors defines cancer gene targets. *Proc Natl Acad Sci USA* **103**: 2257–2261.

Wang D, DuBois RN. (2010). Eicosanoids and cancer. *Nat Rev Cancer* **10**: 181–193.

Webster RJ, Giles KM, Price KJ, Zhang PM, Mattick JS, Leedman PJ. (2009). Regulation of epidermal growth factor receptor signaling in human cancer cells by microRNA-7. *J Biol Chem* **284**: 5731–5741.

Wu H, Sun S, Tu K, Gao Y, Xie B, Krainer AR *et al.* (2010). A splicing-independent function of SF2/ASF in microRNA processing. *Mol Cell* **38**: 67–77.

Yamashita S, Takahashi S, McDonell N, Watanabe N, Niwa T, Hosoya K *et al.* (2008). Methylation silencing of transforming growth factor-β receptor type II in rat prostate cancers. *Cancer Res* **68**: 2112–2121.

Supplementary Information accompanies the paper on the Oncogene website (http://www.nature.com/onc)

Histopathology

Histopathology 2012, 60, E12–E18. DOI: 10.1111/j.1365-2559.2012.04174.x

DNA methyltransferase 3B expression is associated with poor outcome of stage I testicular seminoma

Eri Arai,[1] Tohru Nakagawa,[2] Saori Wakai-Ushijima,[1] Hiroyuki Fujimoto[2] & Yae Kanai[1]

[1]*Division of Molecular Pathology, National Cancer Center Research Institute, and* [2]*Department of Urology, National Cancer Center Hospital, Tokyo, Japan*

Date of submission 12 April 2011
Accepted for publication 14 July 2011

Arai E, Nakagawa T, Wakai-Ushijima S, Fujimoto H & Kanai Y
(2012) *Histopathology* 60, E12–E18

DNA methyltransferase 3B expression is associated with poor outcome of stage I testicular seminoma

Aims: To examine in testicular seminomas the expression of DNA methyltransferase 3B (DNMT3B), which is known to be associated with early embryonic development and carcinogenesis, and to obtain a predictive marker for relapse of stage I seminomas.

Methods and results: Immunohistochemical examination of DNMT3B was performed in 88 cases of seminoma, 35 (39.8%) of which showed widely scattered nuclear immunoreactivity for DNMT3B, and 53 (60.2%) of which were completely negative. The incidence of focal DNMT3B expression was higher in stage III seminomas (5/5, 100%) than in stage I (25/70, 35.7%) or stage II (5/13, 38.5%) seminomas ($P = 0.011$). In stage I seminomas there were no significant correlations between DNMT3B expression and tumour size, invasion of the rete testis, or lymphatic or vascular involvement. Six of 25 cases (24%) showing DNMT3B expression relapsed, whereas only 3/45 cases (6.7%) lacking such expression did so ($P = 0.037$). Patients with seminomas showing DNMT3B expression had a significantly lower relapse-free survival rate than patients whose tumours lacked this feature ($P = 0.0464$).

Conclusions: Patients with seminomas showing focal DNMT3B expression are at increased risk of relapse, and should be followed up carefully.

Keywords: DNA methyltransferase 3B, prognostication, seminoma, testicular germ cell tumour, tumour relapse

Abbreviations: DNMT, DNA methyltransferase; TGCT, testicular germ cell tumour

Introduction

Seminoma is the most common histological subtype of testicular germ cell tumour (TGCT). At initial presentation, approximately 70–80% of patients with seminoma are diagnosed at clinical TNM stage I, i.e. showing no evidence of metastasis. However, 15–20% of them relapse after orchiectomy. As such relapse may occur 5 years or more after orchiectomy,[1] careful long-term follow-up is necessary. However, prolonged follow-up and frequent radiological examinations are burdensome and costly.

Although postoperative radiotherapy of the para-aortic area was the standard choice for several decades,[2] long-term follow-up studies have demonstrated an association of radiotherapy with late complications (i.e. cardiovascular disease[3] and secondary malignancy).[4,5] In recent years, although single-course chemotherapy has yielded survival data equivalent to those after radiotherapy,[6] its associated complications have not yet been evaluated in a long-term follow-up study. To avoid unnecessary treatment or over-frequent surveillance, markers predicting relapse risk are needed.

DNA methylation alterations play an important role in human carcinogenesis.[7] With respect to TGCTs, a difference in methylated genes between seminoma and

Address for correspondence: Y Kanai, Division of Molecular Pathology, National Cancer Center Research Institute, 5-1-1 Tsukiji, Chuo-ku, Tokyo 104-0045, Japan.
e-mail: ykanai@ncc.go.jp

non-seminomatous TGCT has been reported.[8,9] In addition, TGCT originates from male germ cells, and has various histological subtypes resembling the differentiation of fertilized germ cells to embryos. DNA methyltransferase 3B (DNMT3B) is a key enzyme for *de-novo* DNA methylation during the dynamic DNA methylation reprogramming that occurs in early embryogenesis.[10] These facts suggest the possible participation of DNMT3B in TGCT development. However, only an association between DNMT3B expression and drug sensitivity of cultured embryonal carcinoma cells[11] has been reported to date, and no studies have examined the clinicopathological significance of DNMT3B expression in TGCT. In this study, we examined the expression of DNMT3B protein in seminomas and explored the possibility of using it for prognostication.

Materials and methods

PATIENTS AND TISSUE SAMPLES

Eighty-eight testicular seminomas obtained from patients who underwent radical orchiectomy at the National Cancer Center Hospital, Tokyo, Japan were analysed. The mean (±standard deviation) age of the patients was 38.8 ± 9.2 years (range 21–66 years). The pathological diagnosis of TGCT was performed by two pathologists (E.A. and Y.K.), on the basis of the World Health Organization classification.[12]

Initial staging was carried out with a combination of chest X-ray and computed tomography scans. In this cohort, none of the patients received any preoperative therapy for the seminoma. None of the patients with stage I seminomas had received any postoperative therapy until relapse was diagnosed, and they had been under surveillance with chest X-ray, computed tomography scans, and determination of serum tumour marker levels (α-fetoprotein and the β-subunit of human chorionic gonadotropin).

This study was approved by the Ethics Committee of the National Cancer Center, Tokyo, Japan.

ANTIBODY

A polyclonal anti-human DNMT3B antibody was raised by immunizing rabbits with polypeptides corresponding to the C-terminal region of DNMT3B, N-ENKTRRRTADDSATS-C. To confirm the specificity of this antibody, NCC-IT cells, originating from human testicular teratoma,[13] were subjected to western blotting analysis (Figure 1). Total cell extracts were separated by sodium dodecylsulphate (SDS) polyacrylamide gel electrophoresis and transferred electrophoretically to polyvinylidene difluoride (PVDF) filters, which were then incubated with the rabbit anti-human DNMT3B antibody (diluted 1:1000) overnight at 4°C, followed by horseradish peroxidase-linked anti-rabbit immunoglobulin (Amersham Biosciences, Buckinghamshire, UK). Finally, an ECL western blotting detection system (Amersham) was used for detection.

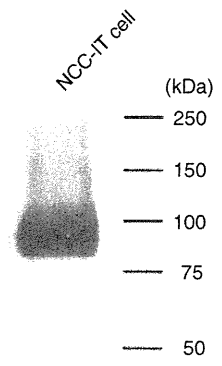

Figure 1. Western blotting with anti-human DNA methyltransferase 3B (DNMT3B) polyclonal antibody. A major immunoreactive band of about 95.8 kDa, corresponding to the molecular mass of DNMT3B, was detected in NCC-IT cells.

IMMUNOHISTOCHEMISTRY

Three-micrometre-thick sections of formalin-fixed, paraffin-embedded tissue specimens of each seminoma were deparaffinized and dehydrated. For antigen retrieval, the sections were heated for 10 min at 120°C in an autoclave. Non-specific reactions were blocked with 2% normal swine serum. All sections were incubated with the rabbit anti-human DNMT3B polyclonal antibody at 4°C overnight, and then with biotinylated secondary antibody (anti-rabbit IgG; dilution 1:200; Vector Laboratories, Burlingame, CA, USA;) at room temperature for 30 min. Following this, the sections were treated with Vectastain Elite ABC reagent (Vector Laboratories), and 3,3′-diaminobenzidine tetrahydrochloride was used as the chromogen. All sections were counterstained with haematoxylin. As a negative control, the primary antibody was omitted from the reaction sequence. Because high-level expression of DNMT3B mRNA has been reported in non-seminomatous TGCT, especially in embryonal carcinoma,[11,14,15] we used three tissue specimens of testicular embryonal carcinoma as positive controls for immunohistochemistry.

STATISTICS

Correlations between focal DNMT3B expression and clinicopathological features were analysed with the

chi-squared test ($P < 0.05$). Survival curves of patients with and without focal DNMT3B expression in their testicular seminomas were calculated by the Kaplan–Meier method, and differences compared using the log-rank test.

Results

DNMT3B EXPRESSION IN TGCT

All three samples of embryonal carcinoma used as positive controls showed diffuse and strong immunoreactivity for DNMT3B (Figure 2A,B). Immunoreactivity was observed in the nuclei, but not in either the cytoplasm or the cell membrane.

In contrast to embryonal carcinomas, most seminomas were completely immunonegative for DNMT3B (Figures 2C,D). However, in some seminomas, tumour cells showing strong nuclear immunoreactivity were scattered among a large majority of tumour cells lacking nuclear immunoreactivity (Figure 2E,F,G).

On the basis of these findings, we considered a seminoma to be positive for (focal) DNMT3B expression when one or more tumour cells per 50 high-power fields showed strong nuclear immunoreactivity equivalent to that of embryonal carcinoma. With the use of this criterion, 35/88 seminomas (39.8%) were considered to be positive. No seminomas showed diffuse immunoreactivity for DNMT3B.

There were no significant morphological differences between the scattered tumour cells showing immunoreactivity and the surrounding tumour cells lacking immunoreactivity in each individual seminoma (Figure 2E,F). Furthermore, there were no significant histological differences between seminomas with focal DNMT3B expression and those lacking it.

CORRELATION BETWEEN FOCAL DNMT3B EXPRESSION AND CLINICOPATHOLOGICAL PARAMETERS OF PATIENTS WITH SEMINOMAS

Table 1 shows the correlation between focal DNMT3B expression and initial tumour stage in patients with seminomas. The incidence of DNMT3B expression was significantly higher in stage III seminomas (100%) than in stage I (35.7%) or stage II (38.5%) seminomas ($P = 0.011$), suggesting that such expression may reflect tumour aggressiveness. Therefore, we analysed the correlation between DNMT3B expression and various clinicopathological parameters in stage I seminomas. There were no significant correlations between expression and tumour size, invasion of the rete testis, invasion of the epididymis, lymphatic or vascular involvement, or invasion of the spermatic cord (Table 2). On the other hand, 9/70 patients with stage I seminoma suffered tumour relapse during follow-up after orchiectomy (metastasis to the retroperitoneal lymph nodes in eight and to the lumbar vertebra and humerus in one). Six of 25 cases (24%) showing DNMT3B expression developed distant metastases, whereas only 3/45 cases (6.7%) lacking expression did so ($P = 0.037$; Table 2).

PROGNOSTIC SIGNIFICANCE OF FOCAL DNMT3B EXPRESSION IN STAGE I SEMINOMA

Figure 3 shows the Kaplan–Meier survival curves of patients with stage I seminomas. The period covered ranged from 15 to 5509 days (mean 1794 days). The relapse-free survival rate of patients with seminomas showing DNMT3B expression was significantly lower than that of patients with seminomas lacking expression ($P = 0.0464$).

Discussion

Postoperative management of stage I seminoma has been the subject of active discussion among clinicians and researchers.[16–18] Although both postoperative radiotherapy and chemotherapy can reduce the rate of relapse in patients with stage I seminomas,[6] patients who do not suffer relapse may be overtreated. As curative chemotherapy is available for metastatic seminoma if it can be detected early, careful surveillance is thought to be an effective strategy for avoiding overtreatment.[17] Estimation of relapse risk may be advantageous for appropriate surveillance planning in individual patients with stage I seminoma.

Several groups have studied prognostic factors in stage I seminoma. On the basis of a pooled analysis, Warde *et al.* reported that tumour size (≤40 mm or >40 mm), invasion of the rete testis and lymphatic or vascular involvement were predictive of relapse on univariate analysis, and that tumour size and invasion of the rete testis remained significant on multivariate analysis.[19,20] However, other papers did not report these factors to be significantly predictive. In our cohort, although lymphatic or vascular involvement was significantly correlated with tumour relapse ($P = 0.0304$), tumour size and invasion of the rete testis were not ($P = 0.1445$ and $P = 0.0566$, respectively, log-rank test). Thus, any prognostic impacts of these clinicopathological parameters are still controversial. Moreover, no significant molecular

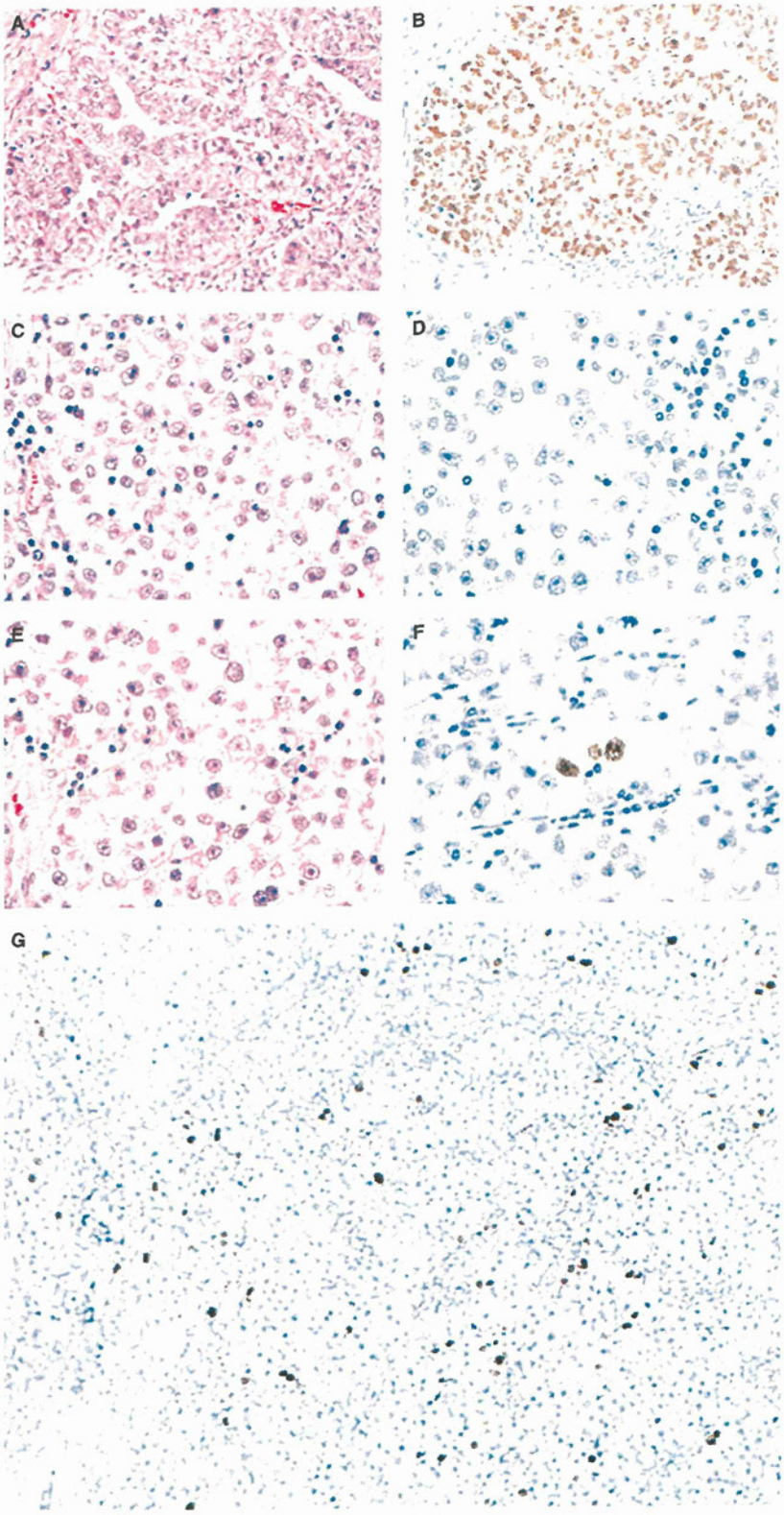

Figure 2. Haematoxylin and eosin staining (A,C,E) and immunohistochemistry with anti-human DNA methyltransferase 3B (DNMT3B) antibody (B,D,F,G) in testicular germ cell tumours. Embryonal carcinomas, as positive controls, showed diffuse and strong nuclear immunoreactivity for DNMT3B (A,B). Fifty-three of 88 seminomas were completely negative for DNMT3B (C,D), and scattered tumour cells with nuclear immunoreactivity were observed in the other 35 seminomas (E,F). DNMT3B-positive cells showed immunoreactivity as strong as that in embryonal carcinoma, whereas the surrounding tumour cells completely lacked immunoreactivity (F). There were no morphological differences between DNMT3B-positive and DNMT3B-negative cells (E,F). Widely scattered nuclear immunoreactivity for DNMT3B was seen at low magnification (G).

Table 1. Correlation between focal DNA methyltransferase 3B (DNMT 3B) expression and initial TNM stage in patients with seminomas

	Focal DNMT3B expression		
Initial TNM stage	Negative	Positive	*P**
Stage I	45	25	0.011
Stage II	8	5	
Stage III	0	5	

*Chi-squared test.

Table 2. Correlations between focal DNA methyltransferase 3B (DNMT3B) expression and clinicopathological parameters in stage I seminomas

	Focal DNMT3B expression		
Clinicopathological parameters	Negative	Positive	*P**
Tumour size (mm)			
≤40	16	8	0.764
>40	29	17	
Invasion of the rete testis†			
Negative	13	10	0.343
Positive	32	15	
Invasion of the epididymis			
Negative	44	24	0.669
Positive	1	1	
Vascular involvement			
Negative	36	15	0.071
Positive	9	10	
Invasion of the spermatic cord			
Negative	44	23	0.253
Positive	1	2	
Tumour relapse			
Negative	42	19	**0.037**
Positive	3	6	

*Chi-squared test.
†All positive cases showed interstitial invasion but not Pagetoid spread.
The *P*-value of <0.05, which indicates significant differences, is in bold.

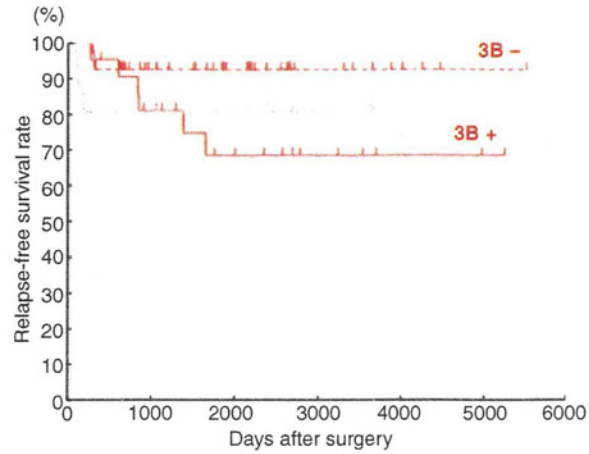

Figure 3. Kaplan–Meier survival curves of patients with stage I testicular germ cell tumours (TGCTs). The relapse-free survival rate of patients with seminomas showing focal DNMT3B expression (red solid line) was significantly lower than that of patients with seminomas not showing this feature (red broken line, $P = 0.0464$). There was no significant difference between the relapse-free survival rate of patients with seminomas showing focal DNMT3B expression and that of patients with non-seminomatous TGCTs (gray line, $P = 0.747$). The time to relapse of patients with seminomas showing DNMT3B expression tended to be longer than that of patients with non-seminomatous TGCTs.

marker for prognostication of patients with seminoma has yet been identified.

In the present study, we found, using immunohistochemistry, that seminomas were separable into two groups on the basis of DNMT3B protein expression: focal DNMT3B expression with widely scattered nuclear reactivity, and absence of such expression. Patients with seminomas showing focal DNMT3B expression were frequently diagnosed at a higher stage (Table 1), and had a poorer outcome (Figure 3), than patients with seminomas lacking such expression.

Tickoo *et al.*[21] suggested that seminomas with 'atypical features', based on morphology, positive expression of CAM5.2 and/or CD30, and negative expression of CD117, tended to be more aggressive, with a higher initial tumour stage. When our cohort of seminomas was examined on the basis of the same methods and criteria,[21] CAM5.2 reactivity (15/87 cases, 17.2%) was significantly correlated with widely scattered nuclear reactivity for DNMT3B ($P = 0.0028$), whereas histological atypia ($P = 0.321$) and expression of CD30 ($P = 0.0653$) and CD117 ($P = 0.0814$) did not show such significant correlations. CAM5.2 reactivity did not correlate significantly with any of the clinicopathological parameters in Table 2, including tumour relapse ($P = 0.949$) or relapse-free survival rate ($P = 0.6300$, log-rank test).

The relapse-free survival rate of patients with seminomas showing focal DNMT3B expression was as low as that of the 16 examined patients with stage I non-seminomatous TGCTs who underwent orchiectomy at the NCCH, Tokyo, Japan ($P = 0.747$; Figure 3), although previously patients with seminomas have been generally considered to have a more favourable outcome than those with non-seminomatous TGCTs.[22,23] Moreover, seminomas showing DNMT3B expression tended to relapse later than non-seminomatous TGCTs (Figure 3). These data indicate that DNMT3B expression may be a potentially useful indicator for estimation of relapse risk in patients with stage I seminoma: patients whose tumours show such expression should be followed up as closely as, and for a longer period than, patients with non-seminomatous TGCTs.

Immunohistochemistry may be the only method capable of detecting widely scattered nuclear reactivity: analyses of mRNA and protein in tissue and serum samples using other methods may not be able to demonstrate DNMT3B expression in only a small number of scattered tumour cells. Thus, immunohistochemistry for DNMT3B, which can be performed on the formalin-fixed, paraffin-embedded tissue specimens prepared for routine pathological diagnosis, may be clinically useful for prognostication of stage I seminomas after prospective validation.

According to the histogenetic model proposed by Srigley *et al.*,[24] seminoma has the potential to differentiate to embryonal carcinoma or other non-seminomatous TGCTs, resembling the differentiation of fertilized germ cells to embryos. In fact, in patients with testicular seminomas who suffer relapse, the metastatic lesions show histological subtypes of embryonal carcinomas and other non-seminomatous TGCTs. *De-novo* DNMT, Dnmt3b, contributes to dynamic epigenetic reprogramming, especially in early mammalian embryogenesis,[10] and is expressed in pluripotent cells, such as the inner cell mass and embryonic ectoderm cells of mouse embryos, and in isolated embryonic stem cells.[25] Embryonal carcinomas also showed high-level expression of DNMT3B (Figure 2A,B).[11,14,15] DNMT3B may be associated with cell pluripotency through its *de-novo* DNA methylation ability, not only during development but also in TGCTs. Focal DNMT3B expression may reflect the potential for differentiation to embryonal carcinomas and other non-seminomatous TGCTs in a proportion of tumour cells in stage I seminoma. It is feasible that seminomas with such potential would relapse as frequently as non-seminomatous TGCTs after a period long enough to allow such differentiation to occur.

References

1. von der Maase H, Specht L, Jacobsen GK *et al.* Surveillance following orchidectomy for stage I seminoma of the testis. *Eur. J. Cancer* 1993; **14**; 1931–1934.
2. NCCN clinical practice guidelines in oncology, testicular cancer, Version 2.2011. Available at: http://www.nccn.org/professionals/physician_gls/f_guidelines.asp
3. Huddart RA, Norman A, Shahibi M *et al.* Cardiovascular disease as a long-term complication of treatment for testicular cancer. *J. Clin. Oncol.* 2003; **21**; 1513–1523.
4. Moller H, Mellemgaard A, Jacobsen GK *et al.* Incidence of second primary cancer following testicular cancer. *Eur. J. Cancer* 1993; **29A**; 672–676.
5. van Leeuwen F, Stiggelbout AM, van den Belt-Dusebout AW *et al.* Second cancer risk following testicular cancer: a follow-up study of 1,909 patients. *J. Clin. Oncol.* 1993; **11**; 415–424.
6. Oliver RT, Mason MD, Mead GM *et al.* MRC TE19 collaborators and the EORTC 30982 collaborators. Radiotherapy versus single-dose carboplatin in adjuvant treatment of stage I seminoma: a randomized trial. *Lancet* 2005; **366**; 293–300.
7. Kanai Y. Genome-wide DNA methylation profiles in precancerous conditions and cancers. *Cancer Sci.* 2010; **101**; 36–45.
8. De Jong J, Weeda S, Gillis AJ *et al.* Differential methylation of the OCT3/4 upstream region in primary human testicular germ cell tumors. *Oncol. Rep.* 2007; **18**; 127–132.
9. Netto GJ, Nakai Y, Nakayama M *et al.* Global DNA hypomethylation in intratubular germ cell neoplasia and seminoma, but not in nonseminomatous male germ cell tumors. *Mod. Pathol.* 2008; **21**; 1337–1344.
10. Okano M, Bell DW, Haber DA *et al.* DNA methyltransferases Dnmt3a and Dnmt3b are essential for *de novo* methylation and mammalian development. *Cell* 1999; **99**; 247–257.
11. Beyrouthy MJ, Garner KM, Hever MP *et al.* High DNA methyltransferase 3B expression mediates 5-aza-deoxycytidine hypersensitivity in testicular germ cell tumors. *Cancer Res.* 2009; **69**; 9360–9366.
12. Woodward PJ, Mostfi FK, Talerman A *et al.* Germ cell tumors. In Eble JN, Sauter G, Epstein J, Sesterhenn IA eds. *World Health Organization classification of tumours. pathology and genetics of tumours of the urinary system and male genital organs.* Lyon: IARC Press, 2004; 221–249.
13. Teshima S, Shimosato Y, Hirohashi S *et al.* Four new human germ cell lines. *Lab. Invest.* 1988; **59**; 328–336.
14. Almstrup K, Hoei-Hansen CE, Nielsen JE *et al.* Genome-wide gene expression profiling of testicular carcinoma in situ progression into overt tumours. *Br. J. Cancer* 2005; **92**; 1934–1941.
15. Biermann K, Heukamp LC, Steger K *et al.* Genome-wide expression profiling reveals new insights into pathogenesis and progression of testicular germ cell tumors. *Cancer Genom. Proteom.* 2007; **4**; 359–367.
16. Chung P, Warde P. Surveillance in stage I testicular seminoma. *Urol. Oncol.* 2006; **24**; 75–79.
17. Pectasides D, Pectasides E, Constantinidou A *et al.* Stage I testicular seminoma: management and controversies. *Crit. Rev. Oncol. Hematol.* 2009; **71**; 22–28.
18. Horwich A, Alsanjari N, A'Hern R *et al.* Surveillance following orchidectomy for stage I testicular seminoma. *Br. J. Cancer* 1992; **65**; 775–778.
19. Warde P, Gospodarowicz M, Banerjee D *et al.* Prognostic factors for relapse in stage I testicular seminoma treated with surveillance. *J. Urol.* 1997; **157**; 1705–1709.

20. Warde P, Specht L, Horwich A *et al.* Prognostic factors for relapse in stage I seminoma managed by surveillance: a pooled analysis. *J. Clin. Oncol.* 2002; **20**; 4448–4452.
21. Tickoo SK, Hutchinson B, Bacik J *et al.* Testicular seminoma: a clinicopathologic and immunohistochemical study of 105 cases with special reference to seminomas with atypical features. *Int. J. Surg. Pathol.* 2002; **10**; 23–32.
22. Jones RH, Vasey PA. Testicular cancer-management of early disease. *Lancet Oncol.* 2003; **4**; 730–737.
23. Bahrami A, Ro JY, Ayala AG. An overview of testicular germ cell tumors. *Arch. Pathol. Lab. Med.* 2007; **131**; 1267–1280.
24. Srigley JR, Mackay B, Toth P *et al.* The ultrastructure and histogenesis of male germ neoplasia with emphasis on seminoma with early carcinomatous features. *Ultrastruct. Pathol.* 1988; **12**; 67–86.
25. Watanabe D, Suetake I, Tada T *et al.* Stage- and cell-specific expression of Dnmt3a and Dnmt3b during embryogenesis. *Mech. Dev.* 2002; **118**; 187–190.

Molecular and Cellular Biology

Higher-Order Chromatin Regulation and Differential Gene Expression in the Human Tumor Necrosis Factor/Lymphotoxin Locus in Hepatocellular Carcinoma Cells

Takehisa Watanabe, Ko Ishihara, Akiyuki Hirosue, Sugiko Watanabe, Shinjiro Hino, Hidenori Ojima, Yae Kanai, Yutaka Sasaki and Mitsuyoshi Nakao

Mol. Cell. Biol. **2012, 32(8):1529. DOI: 10.1128/MCB.06478-11.**
Published Ahead of Print 21 February 2012.

MCB
Journals.ASM.org

Higher-Order Chromatin Regulation and Differential Gene Expression in the Human Tumor Necrosis Factor/Lymphotoxin Locus in Hepatocellular Carcinoma Cells

Takehisa Watanabe,[a,b] Ko Ishihara,[c,e] Akiyuki Hirosue,[a] Sugiko Watanabe,[a] Shinjiro Hino,[a] Hidenori Ojima,[d] Yae Kanai,[d] Yutaka Sasaki,[b] and Mitsuyoshi Nakao[a,e]

Department of Medical Cell Biology, Institute of Molecular Embryology and Genetics, and the Global Center of Excellence Cell Fate Regulation Research and Education Unit,[a] Department of Gastroenterology and Hepatology, Graduate School of Medical Sciences,[b] and Priority Organization for Innovation and Excellence,[c] Kumamoto University, Kumamoto, Japan; Division of Molecular Pathology, National Cancer Center Research Institute, Tokyo, Japan[d]; and Core Research for Evolutional Science and Technology (CREST), Japan Science of Technology Agency, Tokyo, Japan[e]

The three-dimensional context of endogenous chromosomal regions may contribute to the regulation of gene clusters by influencing interactions between transcriptional regulatory elements. In this study, we investigated the effects of tumor necrosis factor (TNF) signaling on spatiotemporal enhancer-promoter interactions in the human *tumor necrosis factor* (*TNF*)/*lymphotoxin* (*LT*) gene locus, mediated by CCCTC-binding factor (CTCF)-dependent chromatin insulators. The cytokine genes *LTα*, *TNF*, and *LTβ* are differentially regulated by NF-κB signaling in inflammatory and oncogenic responses. We identified at least four CTCF-enriched sites with enhancer-blocking activities and a TNF-responsive TE2 enhancer in the *TNF/LT* locus. One of the CTCF-enriched sites is located between the early-inducible *LTα/TNF* promoters and the late-inducible *LTβ* promoter. Depletion of CTCF reduced *TNF* expression and accelerated *LTβ* induction. After TNF stimulation, via intrachromosomal dynamics, these insulators mediated interactions between the enhancer and the *LTα/TNF* promoters, followed by interaction with the *LTβ* promoter. These results suggest that insulators mediate the spatiotemporal control of enhancer-promoter associations in the *TNF/LT* gene cluster.

Chromosomal regions harboring different tissue-specific or cellular-state-specific gene clusters may be influenced by long-range regulatory elements and higher-order chromatin organization (45, 53, 60). Recent studies suggest that transcriptional regulatory elements, such as enhancers, promoters, and chromatin insulators, contribute to gene activation and inactivation via genome accessibility and chromosomal interactions (8, 18). Among these, chromatin insulators are boundary elements that partition the genome into chromosomal subregions, probably through their ability to block interactions between enhancers and promoters when positioned between them (enhancer-blocking effect) (7, 17, 41). However, the precise mechanisms responsible for the enhancer-blocking effect and the relationship with long-range chromatin interactions remain unclear (47, 49). The CCCTC-binding factor CTCF is a highly conserved 11-zinc-finger protein that plays crucial roles at insulator sites (44). CTCF is also reported to function in transcriptional activation (62, 73) and repression (16, 36). In the *IGF2/H19* locus, CTCF binds to the differentially methylated region (DMR) of the *H19* gene to form a predicted chromatin loop structure (6, 22, 42). Genome-wide analyses identified the distribution of the putative CTCF-binding sites and their consensus sequences (4, 27, 28, 69). We and other groups recently determined that CTCF is enriched with cohesin in at least 14,000 sites on the human genome (46, 54, 65). CTCF and cohesin cooperatively form compact chromatin loops, leading to the colocalization of gene promoters and their common enhancer in the human *apolipoprotein* gene locus (40). CTCF has been reported to interact with nuclear substructures (71, 72), chromatin remodeling factors (26, 33), RNA polymerase II (10), and CTCF itself (34, 72), as well as undergoing several posttranslational modifications of the protein (12, 29, 37, 70).

Inflammation involves the activation of a highly coordinated gene expression program (43). The tumor necrosis factor (TNF) superfamily members, TNF (initially termed TNF-α), lymphotoxin α (LTα, also termed TNF-β), and lymphotoxin β (LTβ), are major proinflammatory cytokines that mediate inflammatory responses in autocrine/paracrine manners (63). TNF and LTα form homotrimers and act as soluble ligands for the TNF receptor. In contrast, LTβ forms a heterotrimer with LTα and functions as a membrane-bound ligand for the LTβ receptor. In addition to their physiological roles, the aberrant or unbalanced expression of these cytokines is linked to pathological conditions, such as tissue damage/remodeling (38), metabolic diseases (14, 20), and cancer development (19, 23). Hepatic TNF expression is closely related to steatohepatitis (64), and LTβ expression is significantly involved in liver regeneration (3) and hepatocellular carcinomas (HCCs) (23, 67). The *TNF/LT* genes are clustered within the major histocompatibility complex (MHC) class III region on human chromosome 6p21.3, which is the most gene-dense region of the human genome (68). Interestingly, it is reported that NF-κB does not directly interact with the proximal human *TNF* promoter (9, 15, 59) and that NF-κB activation induced by TNF treatment in-

Received 25 October 2011 Returned for modification 1 December 2011
Accepted 7 February 2012
Published ahead of print 21 February 2012
Address correspondence to Mitsuyoshi Nakao, mnakao@gpo.kumamoto-u.ac.jp.
Supplemental material for this article may be found at http://mcb.asm.org/.

doi:10.1128/MCB.06478-11

fluences expression of the *TNF/LT* genes, resulting in the amplified inflammatory response (25). Several DNase-hypersensitive sites, generally suggestive of the presence of regulatory elements, have been found in the *TNF/LT* locus (5, 50, 56, 58). However, a transcriptional mechanism and higher-order chromatin regulation in the human *TNF/LT* locus are unknown.

Investigation of the *TNF/LT* locus identified at least four CTCF/cohesin-enriched insulators and a TNF-responsive TE2 enhancer in human hepatic cells. These CTCF-bound sequences possessed enhancer-blocking activities, and one of the insulators was located between the early-inducible *LTα/TNF* promoters and the late-inducible *LTβ* promoter. Chromosome conformation capture (3C) analyses determined that after TNF stimulation, these CTCF-bound insulators initially associated with the TE2 enhancer and the *LTα*, *TNF*, and *LTβ* promoters, followed by a persistent interaction with the TC3 insulator, the TE2 enhancer, and the *LTβ* promoter. These late-phase interactions were consistent with the formation of a place in which the late-inducible *LTβ* gene was transcriptionally active. TNF stimulation thus induces dynamic changes in higher-order chromatin organization of the overall locus, together with differential expression of the *TNF/LT* genes. Based on our findings that insulators mediate the spatiotemporal control of enhancer-promoter interactions, we propose a dynamic chromatin conformation model and enhancer-blocking mechanism mediated by insulators in the *TNF/LT* locus.

MATERIALS AND METHODS

Cell culture. Hep3B, HCT116, and HeLa cells were cultured in a 1:1 mixture of Dulbecco's modified Eagle's minimum essential medium and Ham's F-12 nutrient medium (DMEM/F12; Sigma) supplemented with 10% (vol/vol) fetal bovine serum (FBS). NeHepLxHT cells were cultured in DMEM/F12 supplemented with 10% (vol/vol) FBS, 10^{-7} M dexamethasone, 10^{-7} M insulin, and 50 μg/ml G418. For TNF stimulation, Hep3B and NeHepLxHT cells were treated with recombinant human TNF-α (210-TA; R&D Systems) at concentrations of 5 ng/ml and 0.5 ng/ml, respectively. For inhibition of NF-κB signaling, BAY11-7082 (10 μM) was added to the medium for 1 h before treatment of the cells with TNF for 0.5 or 1 h.

ChIP and quantitative PCR (qPCR) analysis. Hep3B and NeHepLxHT cells were cross-linked with 1% formaldehyde at 37°C for 10 min. Crude cell lysates were sonicated to generate DNA fragments of 200 to 500 bp. Chromatin immunoprecipitation (ChIP) was performed with anti-CTCF (07-729; Millipore), anti-RAD21 (ab992; Abcam), anti-acetylated histone H3 (06-599; Millipore), anti-acetylated histone H4 (06-866; Millipore), anti-p65 (sc-372; Santa Cruz), anti-p300 (sc-585; Santa Cruz), or anti-RNA polymerase II (phosphor-S5) antibodies (ab5131; Abcam) or with control rabbit IgG (sc-2027; Santa Cruz) (26). Cells were cross-linked for an additional 10 min when anti-p65 and anti-p300 antibodies were used.

DNA enrichment in ChIP samples was determined using qPCR analysis with an ABI Prism 7300 system (Applied Biosystems) and SYBR green fluorescence. The threshold was set to cross a point where PCR amplification was linear, and the cycle number required to reach the threshold was recorded and analyzed using the Microsoft Excel software program. PCR was performed using precipitated DNA and the input DNA. Primer sequences are listed in Table S1 in the supplemental material. Other antibodies used were anti-lamin A/C (sc-7292; Santa Cruz).

Electrophoretic mobility shift assay (EMSA). The CTCF protein was synthesized using a coupled *in vitro* transcription/translation reaction with the TNT T7 Quick system (Promega), according to the manufacturer's protocol. For supershift assays, the reaction mixture was combined with 1 μl anti-CTCF antibodies (612148; BD Biosciences) (40). The sequences of the probes were as follows: H19 DMR, 5′-TGG CAC GGA ATT GGT TGT AGT TGT GGA ATC GGA AGT GGC CGC GCG GCG GCA GTG CAG GCT CAC ACA TCA CAG CCC GAG CCC GCC CCA ACT-3; TC1, 5′-TCT CCA GCA CTT CTT GCT CAG GCA GTA CCC AAA GGG GCC GCC TGG GAG CAG CAG AGA CCA GGC CCA AAG CTG CGG GCT TAC AAC AGG TTA GCC ATC CCA-3′; TC2, 5′-AGA CCC TGG TGT CCT CTC TGG CCT TAT TTA CTC CTG GTC CTC TGC CAG CCC TGC CAC CAG ATG GCC TTC TAA CTC CTT GGT TGA AAG GCC CAT CTC ATT C-3′; TC3, 5′-CCC GGT ACA GAG AGC TGC GCA GCG TGA CCG AGC GG CCC TGG GGG TCC CCG CCG CCA GGG GGC GCC CGG CCC CGG TAG CCG ACG AGA CAG TAG AGG-3′; TC4, 5′-CTT CAC CCA GGT CTC TCC AGA GAG CCT CAG GCC GCT GCC TTT ACT TAG TTC TGT GTT CAA TGC CAG AAT GCT GCC TCC TAC AGG AAG TCC ACC TGT ATT GCC CAC ACC TCC T-3′; negative control, 5′-TGG CAA AAA GAA AGG ACA GGG CTG CAA GGA GAG TAC AGA CAT GTG CTG GTG AGT GCA CTG TCT GCA TAG TTA CAC CAG AGC ATC TTA TCA ATC AGA AAC TTA TC-3′.

Luciferase reporter assay. The reporter vector pIHLE consisted of the *luciferase* gene driven by the mouse *H19* promoter (−818 to +6 from the transcription start site), simian virus 40 (SV40) enhancer, and a 1.8-kb AatII-HindIII fragment containing the *H19* DMR insulator. The plasmid pIHLIE was constructed by inserting the 1.8-kb *H19* DMR fragment between the *luciferase* gene and the enhancer. pIHLTE plasmids were constructed by inserting fragments of about 200 bp, including TC1, TC2, TC3, and TC4, between the *luciferase* gene and the enhancer (pIHLTE-1F/1R, -2F/2R, -3F/3R, and -4F/4R, respectively). For pIHLET, TC fragments were inserted downstream of the enhancer in pIHLE (pIHLET-1F/1R, -2F/2R, -3F/3R, and -4F/4R). To prepare pIHLTE with mutations (pIHLTE-1 M, -2 M, -3 M, and -4 M), base substitutions were introduced in CTCF consensus sequences at the TC1, TC2, TC3, and TC4 sites using a PCR-based mutagenesis method.

The reporter vector pPL consisted of the *SV40* promoter and the *luciferase* gene and is identical to the pGL3-Promoter vector (Promega). pTPL, pAPL, and pBPL contained the *TNF* promoter (−1044 to +54 from the transcription start site), *LTα* promoter (−924 to +43 from the transcription start site), and *LTβ* promoter (−971 to +12 from the transcription start site), respectively, instead of the *SV40* promoter of pPL. TE1 and TE2 sequences were PCR amplified and inserted upstream of pPL, pTPL, pAPL, and pBPL (pTE1-PL, pTE2-PL, pTE1-TPL, pTE2-TPL, pTE2-APL, and pTE2-BPL). The primer sequences used to prepare the TE1 and the TE2 sequences were as follows: TE1-S, CCT GTG GCT GGA TGA AAT CT; TE1-AS, CCT GGG CAA CAA AGT GAG AC; TE2-S, CCA GGG GAG TTG TGT CTG TAA; TE2-AS, GCA GTT CGG TTC CTT GTT CT.

Reporter vectors (0.05 pmol) were transfected into Hep3B cells (1.0×10^5 cells) in a 12-well plate, using FuGene6 reagent (Roche Applied Science), and analyzed using a luciferase reporter assay system (Promega) after 24 h. For dual luciferase activities (26), values are shown as means and standard deviations of the results from at least three independent experiments.

qRT-PCR. Total RNA was isolated from cultured cells with TRIzol (Invitrogen). The cDNA synthesis used 2 μg of total RNAs that was reverse transcribed using a High Capacity cDNA reverse transcription kit (Applied Biosystems), according to the manufacturer's instructions. Quantitative PCR was performed using an ABI Prism 7300 system (Applied Biosystems) and SYBR green fluorescence. Each experiment was performed at least three times. The relative fold enrichment was quantified by normalization to *β-actin* or *glyceraldehyde-3-phosphate dehydrogenase* (*GAPDH*) gene expression. Primer sequences are listed in Table S1 in the supplemental material.

siRNA-mediated knockdown. Small interfering RNAs (siRNAs) for GL3, CTCF, and Rad21 were used as previously reported (40). RELA silencer select validated siRNA (s11914; Ambion) was used for p65 knockdown. siRNAs were transfected using the Lipofectamine RNAiMAX reagent (Invitrogen) for 48 h.

3C assay. For the chromosome conformation capture (3C) assays (21, 52), formaldehyde-cross-linked chromatin from Hep3B and NeHepLxHT cells was digested with DpnII overnight, followed by ligation with T4 DNA ligase at 16°C for 4 h. To prepare control templates for standard curves, a bacterial artificial chromosome spanning the *TNF/LT* locus RPCI11.C-47E16 was digested with Sau3AI, which is insensitive to Dam methylase, followed by random religation. After reversing the cross-links, genomic DNA was purified by phenol extraction and ethanol precipitation. The ligated products were assessed using qPCR with an ABI Prism 7300 system (Applied Biosystems) and Thunderbird SYBR qPCR Mix (Toyobo). The efficiency of DpnII digestion was evaluated after the entire 3C treatment using qPCR to amplify uncut fragments spanning the DpnII site. More than 80% of the individual restriction sites were digested in these experiments. The 3C-qPCR data were normalized to a loading control, using internal primers located in the *TNF/LT* gene locus. We gained similar results after normalization with internal primers located in *GAPDH* (data not shown). The relative frequencies of interactions between the reference and its physically close site in the control state were finally normalized to 1. Examples of the calculation for relative interacting frequencies are described in Results. Statistical analysis was performed using Student's *t* test for the results of more than three independent experiments. Primer sequences are listed in Table S1 in the supplemental material.

Immunofluorescence analysis. Cultured human cells were fixed with 4% paraformaldehyde in phosphate-buffered saline (PBS) for 10 min at room temperature. Fixed cells were rinsed three times in PBS for 5 min and permeabilized with PBS containing 0.2% Triton X-100 and 0.5% normal goat serum (NGS) for 5 min on ice. Cells were rinsed three times in PBS containing 0.5% NGS for 5 min and then incubated with rabbit anti-p65 (sc-372; Santa Cruz) for 60 min followed by secondary donkey Cy3-conjugated or Alexa Fluor 488-conjugated antibodies for 60 min. Labeled cells were washed three times in PBS for 10 min each. Samples were analyzed using a fluorescence microscope system (Orca-ER1394; Olympus).

Patients and histological assessment. A total of 38 patients (male, 29; female, 9) with HCC, who had undergone tumor resection at the National Cancer Center Hospital, Tokyo, Japan, between May 2003 and December 2005, were enrolled in the present study. The median patient age and follow-up period were 63 years and 1,719 days, respectively. Among the 38 HCC patients, 12 were immunologically positive for hepatitis C virus (HCV) infection, and 16 for persistent hepatitis B virus (HBV) infection (hepatitis B virus surface antigen positive), and 10 were negative for both HCV and HBV infection. Histological examination of noncancerous liver tissue samples revealed findings compatible with chronic hepatitis in 22 and cirrhosis in 9 and no remarkable histological findings in 7. The 38 HCCs were histologically classified into 3 well-differentiated, 27 moderately differentiated, and 8 poorly differentiated tumors. All patients were followed for more than 100 days. Clinical and pathological profiles were obtained from the medical records of the patients. This study was approved by the Ethics Committee of the National Cancer Center, Tokyo, Japan, and written informed consent was obtained from all patients.

IHC. Immunohistochemistry (IHC) for TNF and LTβ was performed using a polymer-based method with the Envision+Dual Link system-horseradish peroxidase [HRP] (DK-2600 Glostrup; Dako). Sources and dilutions of primary antibodies were as follows: anti-TNF-α (ab9579), 1:100, Abcam; anti-LTβ (ab64835), 1:50, Santa Cruz Biotechnology. Formalin-fixed, paraffin-embedded serial tissue sections (4 μm) were placed on silane-coated slides for IHC. Sections cut through the maximum tumor diameter were selected for IHC evaluation. The sections were deparaffinized and rehydrated in xylene and grade-diluted ethanol (50 to 100%) and submerged for 20 min in 0.3% hydrogen peroxide with absolute methanol to block endogenous peroxidase activity. Antigen retrieval for TNF and LTβ was carried out by heating in target retrieval solution (Tris-EDTA buffer, pH 9; Dako Cytomation) at 121°C for 10 min by a pressure cooker. After protein blocking, the sections were incubated with each primary antibody at room temperature for 1 h, followed by incubation with Envision+Dual Link reagent at room temperature for 30 min, and visualized using 3,3-diaminobenzidine tetrahydrochloride as a chromogen. Finally, the sections were counterstained with hematoxylin. Sections were gently rinsed in PBS between incubation steps. The primary antibody was omitted from the reaction sequence as a negative control.

All sections were evaluated by two pathologists, Y. Kanai and H. Ojima, with no knowledge of any clinical or pathological information. Immunoreactivities of TNF and LTβ were defined as follows: negative, no cytoplasmic staining was observed or the intensity of cytoplasmic staining was lower than that for noncancerous hepatocytes within the same section in more than 50% of cancer cells; positive, the intensity of cytoplasmic staining was equivalent to or higher than that of noncancerous hepatocytes in more than 50% of cancer cells.

Statistical analysis. Differences between groups were analyzed using Student's *t* test. A P value of <0.05 was considered statistically significant.

RESULTS

Distribution of CTCF-enriched sites in the human *TNF/LT* gene cluster. CTCF-enriched sites in the human *TNF/LT* gene region were investigated by checking several genome-wide CTCF-binding profiles available on websites and in our published data (40, 65). At least four CTCF-enriched sites (TC1, TC2, TC3, and TC4) were identified in this locus and were conserved among the cells tested (Fig. 1A; see also Fig. S1A in the supplemental material). There were no probe sets for the TC2 site in genome tiling arrays because of the presence of frequent repeat sequences (shown by asterisks in Fig. S1A in the supplemental material). Interestingly, TC3 was located between the *TNF* and *LT*β gene promoters, forming the possible boundary between these adjacent chromosomal subregions.

Based on previous reports (28, 69), each TC site contained a 20-bp consensus CTCF-binding motif (Fig. 1B). To determine if CTCF bound directly to these TC sequences, we performed electrophoretic mobility shift assays (EMSAs) using radiolabeled duplex probes of approximately 100 bp for each TC site and the *in vitro* transcribed/translated CTCF protein. Similar to the DMR insulator of the *H19* gene used as a control (40), the TC probes formed complexes with CTCF and were further supershifted by anti-CTCF antibodies. In contrast, negative-control (NC) probes, which had sequences located downstream of the *NFKBIL1* gene, did not bind to CTCF. In addition, competition assays using mutated TC probes carrying base substitutions within the consensus motif showed that mutated probes did not bind to the CTCF protein (see Fig. S1B and C in the supplemental material), indicating that CTCF specifically bound to the TC sequences.

In order to clarify the localization of CTCF and the cofactor cohesin RAD21 in hepatic cells, we performed chromatin immunoprecipitation (ChIP) analyses using anti-CTCF and anti-RAD21 antibodies, followed by quantitative PCR (qPCR) (Fig. 1C and D). We used standard cell lines: Hep3B, which originates from human HCC, and NeHepLxHT, which is a telomerase-immortalized human neonatal hepatocyte line (51). Both CTCF and RAD21 bound to the TC sites but not to the NC site. RAD21 was relatively enriched with CTCF at TC1 in the *TNF/LT* locus. The CTCF enrichment at the TC sites in Hep3B cells may be remarkable due to the high expression of this gene (see Fig. S1D in the supplemental material) compared with that in NeHepLxHT cells.

Differential regulation of *TNF/LT* genes under TNF stimulation. To examine the transcriptional regulation of the *TNF/LT*

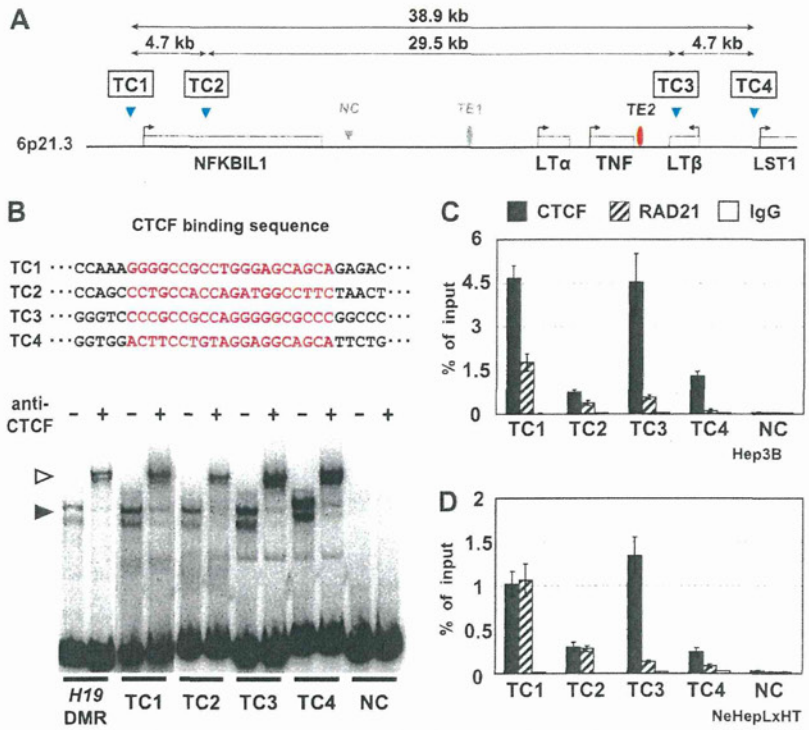

FIG 1 CTCF-enriched sites in the human *TNF/LT* gene cluster locus. (A) CTCF-enriched sites in the *TNF/LT* locus on human chromosome 6p21.3. In addition to the *NFKBIL1*, *LTα*, *TNF*, *LTβ*, and *LST1* genes, a newly identified TE2 enhancer is indicated by a red oval. Based on genome-wide CTCF-binding profiles available from websites and our published data (see Fig. S1A in the supplemental material), four enriched sites were designated TC1, TC2, TC3, and TC4. NC is used as a negative control, and TE1 is a site with no enhancer activity. (B) Direct binding of CTCF to TC sequences. Predicted CTCF-binding sequences within TC1, TC2, TC3, and TC4 sites are indicated, together with the 20-bp consensus motif (red). For EMSAs, radiolabeled duplex probes of approximately 100 bp for each TC site were incubated with anti-CTCF antibodies and synthesized CTCF. Solid and open arrowheads indicate CTCF DNA and the supershifted complexes, respectively. The *H19* DMR insulator and an intergenic unrelated sequence (NC) were used as controls. (C and D) Existence of CTCF and the cofactor cohesin RAD21 at TC sites. Chromatin immunoprecipitation analyses were carried out with anti-CTCF and anti-RAD21 antibodies and control IgG, followed by quantitative PCR with specific primers for each TC site in Hep3B cells (C) or NeHepLxHT cells (D).

genes, we performed quantitative reverse transcription (RT)-PCR (qRT-PCR) analyses with Hep3B and NeHepLxHT cells stimulated by TNF-induced NF-κB activation (Fig. 2A; see also Fig. S2A and B in the supplemental material). Expression of *LTα* and *TNF* mRNAs was markedly increased in Hep3B cells 1 h after stimulation, but *LTβ* mRNA was not simultaneously induced. Moreover, *TNF* expression seemed to be variable after the 1-h peak, while *LTα* and *LTβ* expression did not peak until 24 h after TNF treatment. Early induction of the *LTα* and *TNF* genes also occurred in NeHepLxHT cells, with subsequent expression of the *LTβ* gene. The patterns of *TNF/LT* expression differed between these cell lines, probably due to the constitutively low activation of the NF-κB pathway in Hep3B cells (see Fig. 4A) (11, 55).

Nuclear translocation of NF-κB is critical for its activation (24), and we therefore investigated its subcellular localization under TNF stimulation, using immunofluorescent staining of p65, a subunit of the NF-κB heterodimer (Fig. 2B; see also Fig. S2C in the supplemental material). Cytoplasmic p65 translocated to the nucleus at 30 min after stimulation, and this translocation was inhibited by the addition of BAY11-7082, a specific inhibitor of IκBα phosphorylation (48). The translocated p65 was found to decrease at 1 h after the stimulation (see Fig. S2D in the supplemental material). The expression status of the *TNF/LT* genes was analyzed in parallel using qRT-PCR analyses (Fig. 2C and D). TNF-induced expression of *TNF*, *LTα*, and *LTβ* was attenuated by NF-κB inhibition. Since the use of BAY11-7082 had cytotoxic effects at late time points after TNF stimulation, we carried out siRNA-mediated knockdown of p65 (see Fig. S2G and H in the supplemental material). The induction of the *TNF*, *LTα*, and *LTβ* genes was consistently inhibited by depletion of p65, indicating that the *TNF/LT* genes are regulated by NF-κB in the TNF-treated hepatic cells. Expression of the neighboring *NFKBIL1* gene was unaffected by the stimulation. TNF treatment caused no significant cell damage throughout the study (see Fig. S2E and F in the supplemental material). Thus, the *TNF/LT* genes are differentially induced by TNF-activated NF-κB signaling.

CTCF-dependent enhancer-blocking activity in the *TNF/LT* gene locus. Previous studies demonstrated that the *H19* DMR insulator contains multiple CTCF-binding sites, which are essential for enhancer-blocking activity (6, 22, 26). Luciferase reporter assays were performed with Hep3B cells to test the enhancer-blocking effects of TC1, TC2, TC3, and TC4 (Fig. 3). The presence of TC1, TC2, TC3, and TC4 between the enhancer and promoter reduced the luciferase activities to approximately 60% of those for the control pIHLE vector (pIHLTE-1F, pIHLTE-2F, pIHLTE-3F, and pIHLTE-4F). TC sequences in the opposite direction showed similar results (pIHLTE-1R, pIHLTE-2R, pIHLTE-3R, and pIHLTE-4R), indicating that the TC sites possess enhancer-block-